Chemical Physics 493 (2017) 102–110

Contents lists available at ScienceDirect

Chemical Physics

journal homepage: www.elsevier.com/locate/chemphys

Natural optical activity of *f-f* transitions in $ErAl_3(BO_3)_4$ single crystal

A.V. Malakhovskii *, V.V. Sokolov, I.A. Gudim

Kirensky Institute of Physics, Federal Research Center KSC SB RAS, 660036 Krasnoyarsk, Russian Federation

ARTICLE INFO

Article history:
Received 31 March 2017
In final form 25 June 2017
Available online 27 June 2017

Keywords:
f-f transitions
Natural circular dichroism
Er^{3+} ion

ABSTRACT

Absorption and natural circular dichroism (NCD) spectra of $ErAl_3(BO_3)_4$ single crystal were measured at 90 K in the range of 10,000–28,200 cm^{-1}. The spectra were decomposed on the Lorentz shape components and the natural optical activities (NOA) of *f-f* transitions between Stark components of the ground and excited multiplets were found. The NCD spectra permitted us to find out existence of two non equivalent positions of Er^{3+} ion in one of its excited states, which are due to the local decrease of the crystal symmetry in this state. Very large NOA of a vibronic line was revealed. This phenomenon was accounted for basing on the new quantum mechanical formula for the NOA of electron transitions. The principle difference of the NOA properties of electric dipole allowed and parity forbidden transitions is discussed.

1. Introduction

Natural circular dichroism (NCD) is widely used in study of organic materials. NCD of inorganic compounds and of 4*f* compounds, in particular, was investigated less extensively, (see, e. g., [1–11]). NCD of the erbium containing compounds was studied in Refs. [4,8,11]. Interrelation between optical properties and natural optical activity (NOA) of *f-f* transitions, on the one hand, and structural features of compounds, on the other hand, was discussed in the mentioned works. Recently, a very large NOA (close to unity) of electron-vibrational (vibronic) *f-f* transitions was revealed in $HoAl_3(BO_3)_4$ [12] crystal. Temperature dependences of the integral NOA and magneto-optical activity of *f-f* transitions between multiplets in $ErAl_3(BO_3)_4$ were studied in Ref. [13]. In the present work we study NOA of transitions between Stark components of the ground and excited multiplets and analyze their nature.Different crystals activated by Er^{3+} ions are widely used in solid state lasers. For example, laser generation was obtained in $YAl_3(BO_3)_4$ crystal with admixture of Er^{3+} ions [14–16]). $ErAl_3(BO_3)_4$ single crystal has huntite-like structure with the trigonal space group $R32$ (D_3^7). Such structure has no center of inversion. As a consequence, crystals of this type can be used also as nonlinear active media [17,18]. Some erbium-containing crystals demonstrate up-conversion luminescence. [19–22]. It is worth emphasizing especially Ref. [22] devoted to up-conversion in microcrystals containing Er^{3+} ions. Absorption spectra of the Er doped $YAl(BO_3)_4$ crystals were studied in Refs. [23–26]. Structural and spectroscopic properties of the $ErAl_3(BO_3)_4$ crystal were investigated in Ref. [27]. The spectroscopic properties were analyzed with the help of the Judd-Ofelt theory. As mentioned above, the crystal belongs to the trigonal symmetry class with the space group $R32$, and its lattice constants are: $a = 9.2833(7)$ Å and $c = 7.2234(6)$ Å [27]. The unit cell contains three formula units. Trivalent rare-earth (RE) ions occupy positions of the D_3 symmetry. They are located at the center of trigonal prisms made up of six crystallographically equivalent oxygen ions. The triangles formed by the oxygen ions in the neighboring basal planes are not superimposed on each other but are twisted by a certain angle. Owing to this distortion, the symmetry D_{3h} of the ideal prism is reduced to the symmetry D_3. The AlO_6 octahedrons share edges in such a way that they form helicoidal chains, which run parallel to the C_3 axis and are mutually independent. All Al ions occupy C_2-symmetry positions in the crystal.

2. Experimental details

Single crystals of $ErAl_3(BO_3)_4$ were grown at small overcooling on seeds from the flux 90% mass ($Bi_2Mo_3O_{12} + 2B_2O_3 + 0{,}5Li_2MoO_4$) + 10% mass $ErAl_3(BO_3)_4$. This flux has saturation temperature $T_{sat} = 960$ °C. Details of the growth procedure have been described in Ref. [28]. Earlier the same crystal was grown from another flux [29]. As grown-up crystals had the size of $5 \times 5 \times 7$ mm^3.

Absorption spectra of the crystal were measured by the two beam technique, using an automated spectrophotometer designed on the basis of the diffraction monochromator MDR-2. Circular dichroism spectra were measured using the modulation of the light

* Corresponding author.
E-mail address: malakha@iph.krasn.ru (A.V. Malakhovskii).

http://dx.doi.org/10.1016/j.chemphys.2017.06.011
0301-0104/

wave polarization with piezoelectric modulator [30]). The modulator consists of the plate of fused silica and piezoelectric ceramic element pasted to it. The modulator is a part of the self-contained generator and oscillates with its resonance frequency of about 25 kHz. Linearly polarized light passed through the plate of the fused silica changes its polarization from right to left circular one with the resonance frequency of the modulator. The circularly polarized light passed through the sample acquires a modulation of its intensity due to circular dichroism of the sample. At the light wavelength changing, the photomultiplier direct current level is maintained constant due to the feedback controlled high voltage power supply of the photoelectron multiplier. Thus, alternating current of the photoelectron multiplier at the frequency of modulation is proportional to the circular dichroism. Amplitude of this alternating current is measured and registered by computer. Both absorption and NCD spectra were obtained with the light propagating along the C_3 axis of the crystal (α-polarization). This direction is the optical axis of the crystal. Therefore influence of the linear birefringence of the crystal is excluded. Optical slit with (spectral resolution) was 0.2 nm in the region of 300–600 nm and 0.4 nm in the region of 600–1100 nm. The sensitivity in the measuring of the circular dichroism was 10^{-4}. The sample was put in a nitrogen gas flow cryostat. Accuracy of the temperature measuring was ~1 K. Thickness of the sample was 0.3 mm.

3. Results and discussion

The α-polarized absorption and NCD spectra of transitions $^4I_{15/2} \rightarrow {}^4I_{11/2}$ (A band), $^4I_{9/2}$ (B band), $^4F_{9/2}$ (D band), $^4S_{3/2}$ (E band), $^2H_{11/2}$ (F band), $^4F_{7/2}$ (G band), $^2G_{9/2}$ (K band), $^4G_{11/2}$ (L band), $^4G_{9/2} + {}^2K_{15/2} + {}^2G_{7/2}$ (M + N + O bands) were measured at temperature 90 K (Figs. 1–9). Both absorption and NCD are given in decimal molar extinctions. The capital symbols in Figures and in Table 1 indicate transitions from the lowest level of the ground multiplet, while the lower case characters indicate transitions from the upper states of the ground multiplet. Identification of *f-f* transitions between multiplets was made according to Kaminskii [31]. Identification of the individual absorption lines we made in Ref. [32], basing on π and σ polarized absorption spectra and selection rules of Table 2. In particular, it was shown that the ground state has $E_{1/2}$ symmetry. All transitions are presented in Table 1, including purely π-polarized ones ($E_{3/2} \rightarrow E_{3/2}$) which are not seen in α-polarization. For vibronic transitions (e. g., *f*10), symmetries of electron states and vibrations and energies of vibrations are given. In principle, the shape of NCD spectra should qualitatively repeat

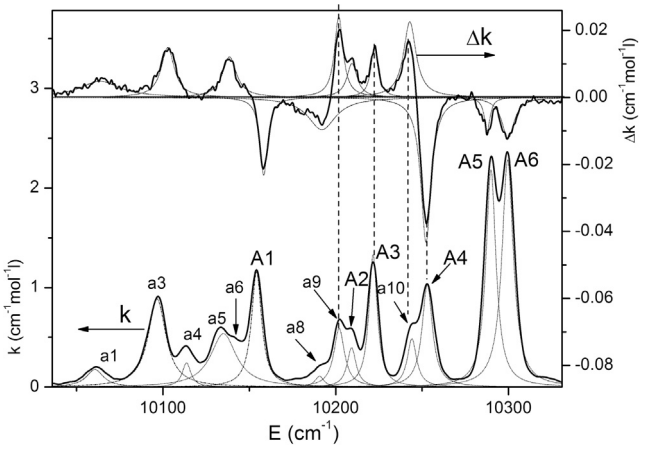

Fig. 1. Absorption (k) and NCD (Δk) spectra of $^4I_{15/2} \rightarrow {}^4I_{11/2}$ transition (A band) at 90 K.

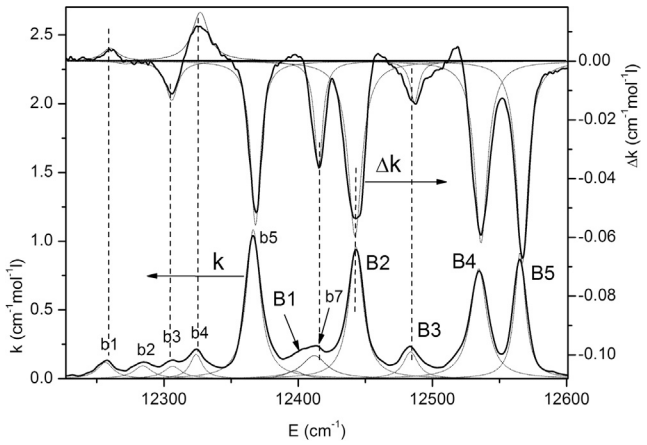

Fig. 2. Absorption (k) and NCD (Δk) spectra of $^4I_{15/2} \rightarrow {}^4I_{9/2}$ transition (B band) at 90 K.

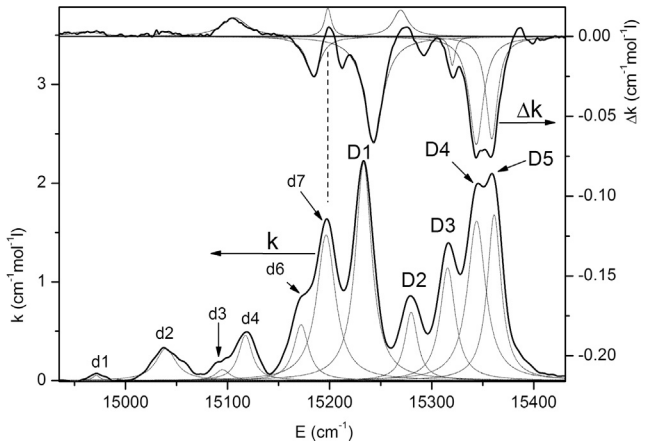

Fig. 3. Absorption (k) and NCD (Δk) spectra of $^4I_{15/2} \rightarrow {}^4F_{9/2}$ transition (D band) at 90 K.

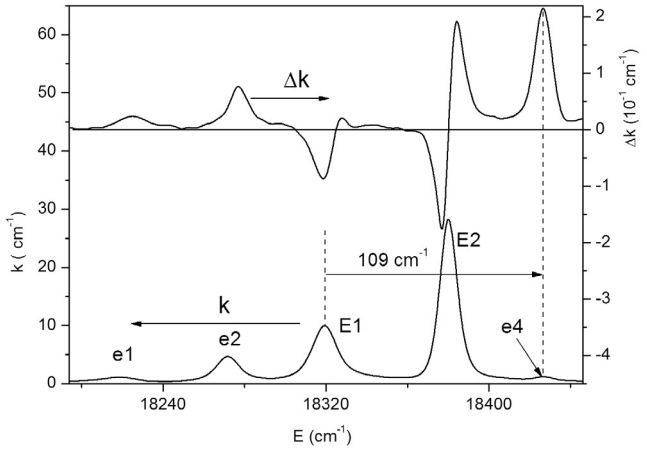

Fig. 4. Absorption (k) and NCD (Δk) spectra of $^4I_{15/2} \rightarrow {}^4S_{3/2}$ transition (E band) at 90 K.

the shape of corresponding absorption spectra but with different signs. However, this is not always so. In particular, in transitions $^4I_{15/2} \rightarrow {}^4G_{11/2}$ (L band) and $^4G_{9/2} + {}^2K_{15/2} + {}^2G_{7/2}$ (M + N + O bands) (Figs. 8 and 9) it was possible to identify only some lines in the NCD spectra and to find their NOA. Below it will be shown that absorption and NCD have not identical nature that can influence the NCD spectra.

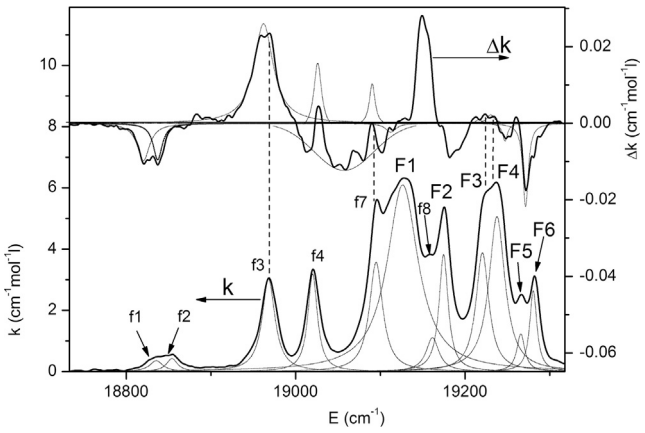

Fig. 5. Absorption (k) and NCD (Δk) spectra of $^4I_{15/2} \rightarrow {}^2H_{11/2}$ transition (F band) at 90 K.

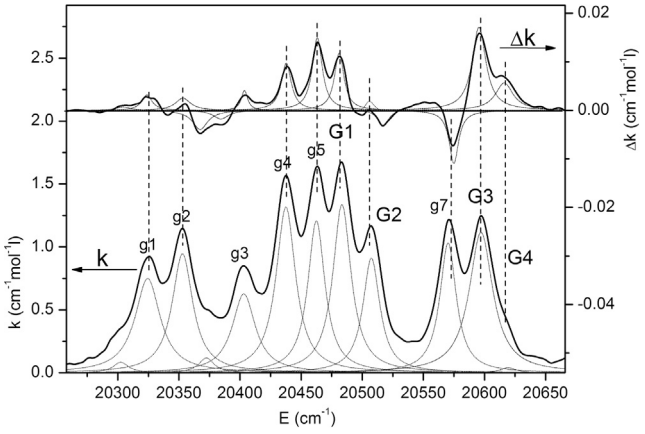

Fig. 6. Absorption (k) and NCD (Δk) spectra of $^4I_{15/2} \rightarrow {}^4F_{7/2}$ transition (G band) at 90 K.

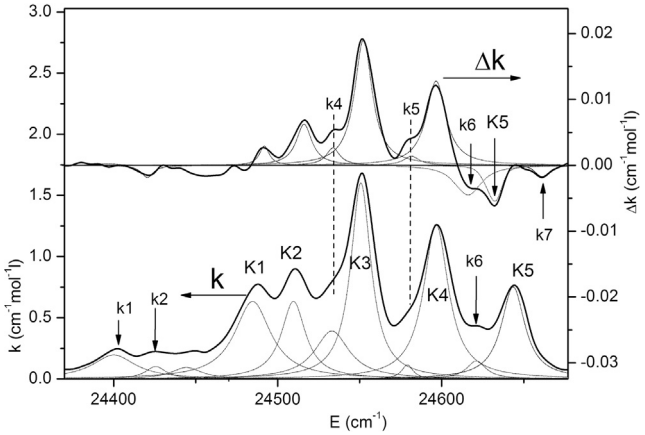

Fig. 7. Absorption (k) and NCD (Δk) spectra of $^4I_{15/2} \rightarrow {}^2G_{9/2}$ transition (K band) at 90 K.

The α-polarized absorption spectra and the NCD spectra (Figs. 1–9) were decomposed on the Lorentz-shape components, where it was possible, and the NOA (dissymmetry factor) of absorption lines were calculated according to the formula:

$$A = \langle \Delta k \rangle_0 / \langle k \rangle_0 = \Delta f / f, \quad (1)$$

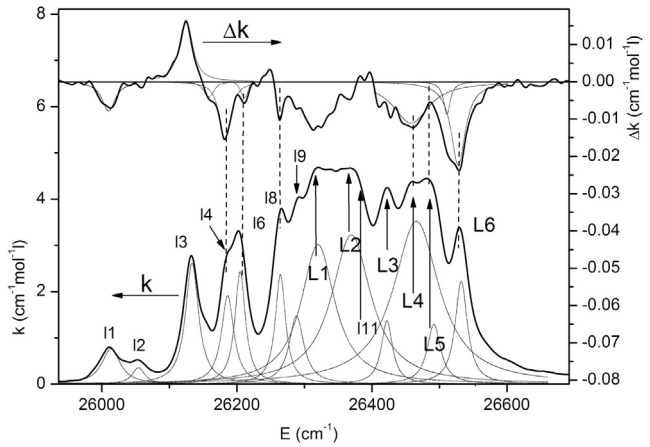

Fig. 8. Absorption (k) and NCD (Δk) spectra of $^4I_{15/2} \rightarrow {}^4G_{11/2}$ transition (L band) at 90 K.

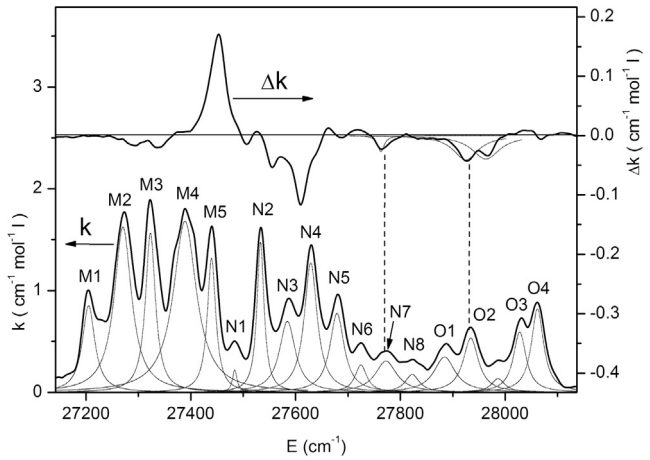

Fig. 9. Absorption (k) and NCD (Δk) spectra of $^4I_{15/2} \rightarrow {}^4G_{9/2} + {}^2K_{15/2} + {}^2G_{7/2}$ transitions (M + N + O bands) at 90 K.

where $\langle \Delta k \rangle_0$ and $\langle k \rangle_0$ are zero moments of the NCD and absorption lines, respectively, and Δf and f are corresponding oscillator strengths. The results are presented in Table 1. In addition to the NOA of the individual transitions, the integral NOA of absorption bands at room temperature based on the data of Ref. [13] are given in Table 3. The integral NOA strongly depend on temperature [13]. Therefore they are given at room temperature since in this case the Stark components of the ground state are more equally populated.

There were made a number of attempts, both experimental [3,10,11] and theoretical [33–35], to find correlation between the quantum numbers L, S and J or their changes during f-f transitions and the NOA. Following the Richardson's theory [33], based on the theory of Ref. [36], we classified transitions studied in the present work according to changes of L, S and J numbers. However, we did not find correlation of results presented in Table 3 with predictions of Ref. [33]. The same conclusion refers to data of Ref. [37] for $Nd_{0.5}Gd_{0.5}Fe_3(BO_3)_4$ crystal.

It is worth considering transition $^4I_{15/2} \rightarrow {}^4S_{3/2}$ (E-band) separately (Fig. 4). Two features were found out in its spectra. The NCD spectrum of the E2 line testifies that a splitting of this line to lines with the opposite signs of NCD takes place. With the help of the decomposition procedure the splitting was found to be of about 5 cm^{-1}. The splitting of the Kramers doublets is impossible. Consequently, the observed phenomenon can be referred to the existing of two kinds of absorbing centers with the opposite signs

Table 1
Parameters of absorption lines: energy (E), width (W), oscillator strength (f), NCD (Δf) and NOA (A).

Exc. state	Symbol	Transition	E (cm^{-1})	W (cm^{-1})	f (10^{-7})	Δf (10^{-9})	A
$^4I_{11/2}$	A1	$E_{1/2} \rightarrow E_{3/2}$	10153	7.19	0.579	−0.869	−0.015
	A2	$E_{1/2} \rightarrow E_{3/2}$	10207	6.29	0.173	0.502	0.029
	A3	$E_{1/2} \rightarrow E_{1/2}$	10220	5.81	0.537	0.515	0.00955
	A4	$E_{1/2} \rightarrow E_{1/2}$	10252	7.19	0.513	−2.19	−0.0427
	A5	$E_{1/2} \rightarrow E_{1/2}$	10290	7.05	1.06	−0.282	−0.00264
	A6	$E_{1/2} \rightarrow E_{1/2}$	10299	7.9	1.25	−0.721	−0.00575
	a1	$E_{1/2} \rightarrow E_{1/2}$	10061	12	0.146	0.882	0.0604
	a2	$E_{3/2} \rightarrow E_{3/2}$	10091		No	No	No
	a3	$E_{3/2} \rightarrow E_{1/2}$	10098	11.4	0.705		
	a4	$E_{1/2} \rightarrow E_{3/2}$	10113	6.63	0.117		
	a5	$E_{3/2} \rightarrow E_{1/2}$	10135	17.5	0.647		
	a6	$E_{1/2} \rightarrow E_{1/2}$	10142				
	a7	$E_{3/2} \rightarrow E_{3/2}$ ($E_{3/2}$ + 84(A_2))	10172		No	No	No
	a8		10190	6.29	0.0482		
	a9	$E_{1/2} \rightarrow E_{1/2}$	10202	7.44	0.305	1.01	0.0331
	a10	$E_{3/2} \rightarrow E_{1/2}$	10244	6.48	0.221	1.36	0.0616
$^4I_{9/2}$	B1	$E_{1/2} \rightarrow E_{1/2}$	12396				
	B2	$E_{1/2} \rightarrow E_{3/2}$	12444	12.5	0.842	−5.08	−0.0604
	B3	$E_{1/2} \rightarrow E_{1/2}$	12483	12.9	0.178	−0.766	−0.043
	B4	$E_{1/2} \rightarrow E_{3/2}$	12534	14.3	0.791	−4.85	−0.0614
	B5	$E_{1/2} \rightarrow E_{1/2}$	12564	9.93	0.607	−4.88	−0.0803
	b1	$E_{1/2} \rightarrow E_{1/2}$	12253	14.3	0.114	0.452	0.0395
	b2	$E_{1/2} \rightarrow E_{1/2}$	12283	16.4	0.104		
	b3	$E_{1/2} \rightarrow E_{3/2}$	12300	16	0.098	−1.03	−0.105
	b4	$E_{3/2} \rightarrow E_{1/2}$	12323	11.2	0.136	1.72	0.126
	b5	$E_{3/2} \rightarrow E_{1/2}$	12364	12.5	0.928	−3.44	−0.037
	b6	$E_{1/2} \rightarrow E_{1/2}$	12375				
	b7	$E_{3/2} \rightarrow E_{1/2}$	12407	22.66	0.236	−1.86	0.07894
$^4F_{9/2}$	D1	$E_{1/2} \rightarrow E_{3/2}$	15231	19.1	2.91	−9.97	−0.0343
	D2	$E_{1/2} \rightarrow E_{1/2}$	15279	15.2	0.729	2.04	0.028
	D3	$E_{1/2} \rightarrow E_{3/2}$	15313	18	1.42	−0.815	−0.00576
	D4	$E_{1/2} \rightarrow E_{1/2}$	15337	21.5	2.38	−7.66	−0.0322
	D5	$E_{1/2} \rightarrow E_{1/2}$	15357	16.5	1.9	−5.97	−0.0315
	d1	$E_{1/2} \rightarrow E_{3/2}$	14964	8.01	0.0295		
	d2	$E_{1/2} \rightarrow E_{1/2}$	15040	23.8	0.525		
	d3	$E_{1/2} \rightarrow E_{1/2}$	15090	16.9	0.13		
	d4	$E_{1/2} \rightarrow E_{3/2}$	15119	16.1	0.513		
	d5	$E_{3/2} \rightarrow E_{3/2}$	15147		No	No	No
	d6	$E_{3/2} \rightarrow E_{1/2}$	15173	17.5	0.685	−2.85	−0.0416
	d7	$E_{1/2} \rightarrow E_{3/2}$	15198	22.2	2.25	0.967	0.00431
	d8	$E_{3/2} \rightarrow E_{3/2}$	15218		No	No	No
	d9	$E_{3/2} \rightarrow E_{3/2}$	15383		No	No	No
$^4S_{3/2}$	E1	$E_{1/2} \rightarrow E_{1/2}$	18322	12.4	0.954	−0.582	−0.0061
	E2a	$E_{1/2} \rightarrow E_{3/2}$	18380	7.45	0.957	−1.91	−0.0199
	E2b	$E_{1/2} \rightarrow E_{3/2}$	18385	7.45	0.957	2.11	0.022
	e1	$E_{1/2} \rightarrow E_{1/2}$	18224	14.9	0.0787	0.237	0.0304
	e2	$E_{3/2} \rightarrow E_{1/2}$	18274	12.4	0.365	0.676	0.0185
	e3	$E_{3/2} \rightarrow E_{3/2}$	18332		No	No	No
	e4	$E_{1/2} \rightarrow E_{1/2}$ ($E_{1/2}$ + 109 (E))	18428	7.45	0.0407	1.36	0.335
$^2H_{11/2}$	F1	$E_{1/2} \rightarrow E_{1/2}$	19138	44.4	18.02		
	F2	$E_{1/2} \rightarrow E_{1/2}$	19174	13	3.43		
	F3	$E_{1/2} \rightarrow E_{3/2}$	19224	18.5	4.88		
	F4	$E_{1/2} \rightarrow E_{3/2}$	19236	22.9	7.77		
	F5	$E_{1/2} \rightarrow E_{1/2}$	19267	11.4	0.96		
	F6	$E_{1/2} \rightarrow E_{1/2}$	19281	10.2	1.84		
	f1		18828	18.5	0.442	−1.17	−0.0265
	f2		18853	15.8	0.457	−0.855	−0.0187
	f3	$E_{1/2} \rightarrow E_{1/2}$	18969	18.2	3.78	3.87	0.0103
	f4	$E_{1/2} \rightarrow E_{1/2}$	18019	13.4	2.96	0.646	0.0022
	f5	$E_{3/2} \rightarrow E_{3/2}$	19065		No	No	No
	f6	$E_{3/2} \rightarrow E_{3/2}$	19081		No	No	No
	f7	$E_{3/2} \rightarrow E_{1/2}$	19092	19	4.67	0.256	0.00055
	f8	$E_{1/2} \rightarrow E_{1/2}$	19159	18.4	1.4		
	f9	$E_{3/2} \rightarrow E_{3/2}$	19187		No	No	No
	f10	$E_{3/2} \rightarrow E_{3/2}$ ($E_{1/2}$ + 131(E))	19367		No	No	No
$^4F_{7/2}$	G1	$E_{1/2} \rightarrow E_{1/2}$	20481	18.4	1.67	0.766	0.0046
	G2	$E_{1/2} \rightarrow E_{1/2}$	20509	16.8	1.05	−0.269	−0.00255
	G3	$E_{1/2} \rightarrow E_{3/2}$	20597	23.7	1.75	1.61	0.0092
	G4	$E_{1/2} \rightarrow E_{1/2}$	20615	15.3	0.0404	0.676	0.168
	g1	$E_{1/2} \rightarrow E_{1/2}$	20328	24.7	1.23	0.224	0.00181
	g2	$E_{1/2} \rightarrow E_{1/2}$	20352	20.5	1.31	0.26	0.00198
	g3	$E_{1/2} \rightarrow E_{1/2}$	20403	23.2	0.973	0.179	0.00185

(*continued on next page*)

Table 1 (*continued*)

Exc. state	Symbol	Transition	E (cm^{-1})	W (cm^{-1})	f (10^{-7})	Δf (10^{-9})	A
	g4	$E_{1/2} \rightarrow E_{1/2}$	20436	19	1.74	0.663	0.00381
	g5	$E_{3/2} \rightarrow E_{1/2}$	20463	17.4	1.41	1.02	0.00725
	g6	$E_{3/2} \rightarrow E_{3/2}$	20548		No	No	No
	g7	$E_{3/2} \rightarrow E_{1/2}$	20571	16.3	1.18	−0.708	−0.00598
$^2G_{9/2}$	K1	$E_{1/2} \rightarrow E_{3/2}$	24481	26.8	1.13	0.143	0.00128
	K2	$E_{1/2} \rightarrow E_{1/2}$	24506	17.9	0.772	0.493	0.0064
	K3	$E_{1/2} \rightarrow E_{1/2}$	24547	15	1.65	1.68	0.0102
	K4	$E_{1/2} \rightarrow E_{3/2}$	24592	18.2	1.56	1.24	0.00795
	K5	$E_{1/2} \rightarrow E_{3/2}$	24638	17.3	0.876		
	k1	$E_{1/2} \rightarrow E_{1/2}$	24387	31.9	0.385		
	k2	$E_{1/2} \rightarrow E_{1/2}$	24415	15	0.102	−0.112	−0.0109
	k3	$E_{3/2} \rightarrow E_{3/2}$	24499		No	No	No
	k4	$E_{1/2} \rightarrow E_{1/2}$	24535	25.5	0.671	0.184	0.00271
	k5	$E_{1/2} \rightarrow E_{1/2}$	24577	8.33	0.0665	0.108	0.0165
	k6	$E_{1/2} \rightarrow E_{1/2}$	24620	14.2	0.143	0.0968	0.00677
	k7		24660	10.9		−0.1	
$^4G_{11/2}$	L1	$E_{1/2} \rightarrow E_{3/2}$	26308				
	L2	$E_{1/2} \rightarrow E_{1/2}$	26357				
	L3	$E_{1/2} \rightarrow E_{1/2}$	26420				
	L4	$E_{1/2} \rightarrow E_{3/2}$	26456				
	L5	$E_{1/2} \rightarrow E_{1/2}$	26487				
	L6	$E_{1/2} \rightarrow E_{1/2}$	26527	22	3.33	−3.68	−0.011
	l1	$E_{1/2} \rightarrow E_{3/2}$	26007	33	1.35	−1.06	−0.008
	l2	$E_{1/2} \rightarrow E_{3/2}$	26052				
	l3	$E_{1/2} \rightarrow E_{1/2}$	26129	23.3	4.2	2.35	0.0056
	l4	$E_{3/2} \rightarrow E_{1/2}$	26181	22.4	2.95	−2.8	−0.0095
	l5	$E_{3/2} \rightarrow E_{3/2}$	26189				
	l6	$E_{1/2} \rightarrow E_{3/2}$	26199	18.45	3.03	−0.4	−0.0013
	l7	$E_{3/2} \rightarrow E_{3/2}$ ($E_{3/2}$ + 81(A_2))	26235		No	No	No
	l8	$E_{3/2} \rightarrow E_{1/2}$	26262				
	l9	$E_{3/2} \rightarrow E_{1/2}$	26289				
	l10	$E_{3/2} \rightarrow E_{3/2}$	26302				
	l11	$E_{1/2} \rightarrow E_{1/2}$	26378				
	l12	$E_{3/2} \rightarrow E_{3/2}$ ($E_{1/2}$ + 156 (E))	26601		No	No	No
	l13	$E_{3/2} \rightarrow E_{3/2}$ ($E_{1/2}$ + 148 (E))	26628		No	No	No
$^4G_{9/2} + {}^2K_{15/2} + {}^2G_{7/2}$	M1	$E_{1/2} \rightarrow E_{3/2}$	27202	29	1.66		
	M2	$E_{1/2} \rightarrow E_{1/2}$	27273	40	4.35		
	M3	$E_{1/2} \rightarrow E_{1/2}$	27323	23	2.46		
	M4	$E_{1/2} \rightarrow E_{1/2}$	27392	53.3	5.92		
	M5	$E_{1/2} \rightarrow E_{3/2}$	27439	19.5	1.76		
	N1	$E_{1/2} \rightarrow E_{1/2}$	27484	10.6	0.162		
	N2	$E_{1/2} \rightarrow E_{1/2}$	27533	16.1	1.62		
	N3	$E_{1/2} \rightarrow E_{3/2}$	27588	36.5	1.66		
	N4	$E_{1/2} \rightarrow E_{1/2}$	27628	29.8	2.55		
	N5	$E_{1/2} \rightarrow E_{3/2}$	27680	32.8	1.73		
	N6	$E_{1/2} \rightarrow E_{1/2}$	27723	27.4	0.503		
	N7	$E_{1/2} \rightarrow E_{3/2}$	27770	49.6	1.02	−2.846	−0.0278
	N8	$E_{1/2} \rightarrow E_{1/2}$	27824	33	0.397		
	O1	$E_{1/2} \rightarrow E_{3/2}$	27888	49	1.14		
	O2	$E_{1/2} \rightarrow E_{1/2}$	27933	35.3	1.27	−8.834	−0.0693
	O3	$E_{1/2} \rightarrow E_{1/2}$	28030	29.2	1.16		
	O4	$E_{1/2} \rightarrow E_{1/2}$	28061	28.1	1.54		

Table 2
Selection rules for electric dipole transitions in D_3 symmetry.

	$E_{1/2}$	$E_{3/2}$
$E_{1/2}$	π, $\sigma(\alpha)$	$\sigma(\alpha)$
$E_{3/2}$	$\sigma(\alpha)$	π

of the NCD. Discussed splitting is observed only on one transition. Consequently, this phenomenon occurs only in the definite excited state and has the local character. In the huntite structure of $R32$ space symmetry rare earth ions occupy three equivalent positions of the D_3 local symmetry in the unit cell. At the lower space symmetry $P3_121$ the local symmetry of the rare earth ions decreases to C_2 one [38] but positions remain equivalent. However it is known, that the unit cell of huntit structure can have also the $C2$ space symmetry [39]. In the unit cell of this space symmetry there are two non-equivalent positions of the rare earth ions with the C_1 local symmetry.

The second feature of the E-band is the very large NOA of the very weak e4-line (Fig. 4, Table 1). Such large NOA of the e4-line testifies, first of all, that mainly twins of the identical chirality exist in the crystal. This line is the vibrational satellite of the E1 electron line, created by a vibration of the E-symmetry [13] with the energy of 109 cm^{-1}. Even larger NCD (close to unity) was observed on the vibronic line in the $HoAl_3(BO_3)_4$ crystal [12]. The k7 resonance on the NCD spectrum (Fig. 7), which is not discerned on the absorption spectrum, also probably refers to a vibronic transition. There are some other vibronic lines in the $ErAl_3(BO_3)_4$, such as a7, f10, l7, l12, l13 (Table 1, [32]), but they are connected with the electron transitions from the upper components of the ground multiplet and correspond to $E_{3/2} \rightarrow E_{3/2}$ transitions. These transitions have

Table 3
Oscillator strengths (f), integral NCD (Δf), integral NOA (A) of f-f absorption bands at room temperature.

Symbol	Excited state	$f\,(10^{-7})$	$\Delta f\,(10^{-9})$	A
A	$^4I_{11/2}$	7.926	7.926	0.010
B	$^4I_{9/2}$	5.105	−6.135	−0.012
D	$^4F_{9/2}$	24.49	−1.880	−0.00077
E	$^4S_{3/2}$	4.433	2.552	0.0058
F	$^4H_{11/2}$	92.38	−8.866	−0.00096
G	$^4F_{7/2}$	213.7	18.58	0.00087
K	$^4G_{9/2}$	9.807	1.079	0.0011
L	$^4G_{11/2}$	114.5	29.73	0.0026
M,N,O	$^4G_{9/2} + {}^2K_{15/2} + {}^2G_{7/2}$	48.03	0.899	0.00019

purely π-polarization and therefore they are not observed in α-polarization. The NOA of the majority of the observed absorption lines (Table 1) are of the same order of magnitude as those in another Er^{3+} compounds [4,8,11]. However, extraordinary large NOA of the vibronic lines should be explained.

The traditional theory of the NCD [36] gives the following expression for the NOA (dissymmetry factor) of a transition $i \to f$

$$A = \mathrm{Im}[\langle i|\vec{d}|f\rangle\langle f|\vec{m}|i\rangle]/|\langle i|\vec{d}|f\rangle|^2. \tag{2}$$

Here Im denotes the imaginary part of a quantity, $\vec{d}$ and $\vec{m}$ are the electric and magnetic dipole moments, respectively. It is supposed in (2) that intensity of the transition is provided by the electric dipole absorption. The formula (2) was obtained for a sample composed of randomly oriented chiral systems, however, majority of researches use it for crystals as well. This formula lies in the background of a number of the subsequent theoretical works (see, e.g., [1,33–35,40–45] and references therein). According to Eq. (2), none of the electron transitions can be almost completely circularly polarized, as it takes place with the e4 transition (Fig. 4, Table 1) and in Ref. [12], since this would require equality of matrix elements of the electric and magnetic dipole moments. Additionally, according to the phenomenological theory, the formula for the NOA should contain the light wave number. Thus, the space dispersion should be taken into account [46,47].

According to the Onsager principle, the electric polarizability tensor follows the relation: $\alpha_{nm}(\vec{k}) = \alpha_{mn}(-\vec{k})$, where $\vec{k}$ is the light wave vector which characterizes the space dispersion. Consequently, the tensor can be decomposed into symmetric and anti symmetric parts. The symmetric part is the even function of $\vec{k}$ and the anti symmetric part is the odd function of $\vec{k}$. If a crystal has the center of inversion, then the anti symmetric part is equal to zero, since vector $\vec{k}$ change sign as a result of the space inversion. If there is no absorption, then α_{mn} is the Hermitian tensor and, consequently, the symmetric components are the real and anti symmetric ones are the imaginary values. If the light propagates along the z-axis, which is simultaneously the optical axis of the crystal, then the symmetric tensor is the diagonal one, but anti symmetric tensor has only components $\alpha_{xy} = -\alpha_{yx}$. Just these components give rise to the natural circular dichroism and birefringence: $\alpha_+ - \alpha_- = g = i\alpha_{xy}$, where α_+ and α_- are polarizabilities for (+) and (−) circularly polarized waves. It is important to note, that in order to describe the circular dichroism and birefringence basing on the Maxwell equations, it is enough, if only the electric polarizability tensor differs from zero and depends on $\vec{k}$. Thus, it is not necessary to take into account magnetic dipole transitions probability, when the electron transition has certainly electric dipole character.

Basing on results of Ref. [46], it is possible to write down the electric polarizability tensor of a molecule corresponding to the electron transition $i \to f$ in the form:

$$\alpha_{nm}(\omega,\vec{k}) \sim \left[\frac{M^n_{if}(-\vec{k})M^m_{fi}(\vec{k})}{\omega_{if}+\omega} + \frac{M^n_{fi}(-\vec{k})M^m_{if}(\vec{k})}{\omega_{if}-\omega}\right] \tag{3}$$

Here $\hat{M}(\vec{k}) = \hat{p}e^{\vec{r}} + e^{i\vec{k}\vec{r}}\hat{p}$ and $\hat{p} = -i\hbar\frac{\partial}{\partial\vec{r}}$, that is, the space dispersion was taken into account. The perturbation inducing the electron transition is: $\hat{U} \sim \vec{E}_0(\hat{M}(\vec{k})e^{-i\omega t} + \hat{M}^*(\vec{k})e^{i\omega t})$, where $\vec{E}_0$ is the amplitude of the light wave electric field. Consequently, at $k = 0$ operator $\hat{M}(\vec{k}=0) = 2\hat{p}$ is proportional to the electric dipole operator. Taking into account that $M_{if} = M^*_{fi}$, it is possible to obtain from (3):

$$\alpha_{nm}(\omega,\vec{k}) \sim \frac{\omega_{if}\mathrm{Re}\left[M^n_{if}(-\vec{k})M^m_{fi}(\vec{k})\right] + i\omega\mathrm{Im}\left[M^n_{if}(-\vec{k})M^m_{fi}(\vec{k})\right]}{\omega^2_{if}-\omega^2}. \tag{4}$$

Formula (3) was obtained in assumption that there is no absorption. Therefore, according to the phenomenological theory, the first term in (4) gives the symmetric part of the polarizability tensor and the second one gives the anti symmetric part (gyration tensor), responsible for the circular birefringence and dichroism. In order to transfer to the resonance region, it is necessary to replace function $1/(\omega^2_{if}-\omega^2)$ by the complex Lorentz function: $1/[(\omega^2_{if}-\omega^2) - i\gamma\omega]$, where γ is the line width. The imaginary part of the function will give dispersion of absorption and dichroism.

Since $e^{i\vec{k}\vec{r}} \approx 1 + i\vec{k}\vec{r}$, we can write

$$\hat{M}(\vec{k}) \approx 2\hat{p} + i(\hat{p}\vec{k}\vec{r} + \vec{k}\vec{r}\hat{p}) = 2\hat{p} + ik(\hat{p}r_k + r_k\hat{p}) \equiv 2\hat{p} + k\Delta\hat{p}. \tag{5}$$

Here r_k is the projection of $\vec{r}$ on the $\vec{k}$ direction. Substituting (5) into (4) we obtain for the value in the brackets:

$$[\ldots] = 4p^n_{if}p^{m*}_{if} + 2k(\Delta p^{m*}_{if}p^n_{if} - \Delta p^n_{if}p^{m*}_{if}) - k^2\Delta p^n_{if}\Delta p^{m*}_{if}. \tag{6}$$

It is possible to show that the second term in (6) is always imaginary one. Therefore and also because this term is proportional to k, it is responsible for the anti symmetric components of the polarizability tensor. In experiments the light usually propagates along the optical axis of the crystal. Let it be z-axis. In this case, as mentioned above, the symmetric part of the polarizability tensor is the diagonal one and the anti symmetric components are $\alpha_{xy} = -\alpha_{yx}$. Additionally $r_k = z$ and according to (5)

$$\Delta\hat{p}^{x,y} = i(\hat{p}^{x,y}z + z\hat{p}^{x,y}). \tag{7}$$

Due to the axial symmetry, matrix elements of the x and y components of the operators are identical that is reflected in double superscripts in (7). Then we obtain:

$$[\ldots] = 4|p^x_{if}|^2 + 2k(\Delta p^{x*}_{if}p^x_{if} - \Delta p^x_{if}p^{x*}_{if}) - k^2|\Delta p^x_{if}|^2. \tag{8}$$

Thus, the NOA of the transition $i \to f$ is:

$$A = \frac{\mathrm{Im}2k(\Delta p^{x*}_{if}p^x_{if} - \Delta p^x_{if}p^{x*}_{if})}{4|p^x_{if}|^2 - k^2|\Delta p^x_{if}|^2}. \tag{9}$$

A difference in the frequency dependencies of α_{xy} and α_x, which is appreciable only far from the resonance, is not taken into account in (9).

If a crystal has the center of inversion and the electric dipole transition is parity allowed, then the matrix element p_{if}^x is not zero, but the matrix element Δp_{if}^x is equal to zero, since according to (7) $\Delta\hat{p}$ is the even function. Thus, the crystal must not have the center of inversion in order to have the NCD, in agreement with the phenomenological theory, and for the allowed transition from (9) we find:

$$A \sim kr = \frac{r}{\lambda}, \tag{10}$$

where r is the radius of the object, absorbing the quantum of the light and λ is the light wave length. Additionally, the NOA is, evidently, proportional to deviation of the local symmetry from the centrosymmetrical one.

Another situation takes place for the electric dipole parity forbidden *f-f* transitions. In this case the absence of the center of inversion is necessary for allowance of the transitions themselves. If there is the center of inversion, the matrix element Δp_{if}^x, responsible for the NCD, on the contrary, is not zero for *f-f* transitions, and it weakly depends on the noncentro-symmetrical distortions. When these distortions decrease the matrix elementp_{if}^x tents to zero but Eq. (9) increases. Thus, it is possible to expect, that NOA of the parity forbidden electric dipole *f-f* transitions can be larger than that of the parity allowed ones. Indeed, the radius of the rare earth ions is of the order of 0.1 nm. Then according to (10) the NOA of allowed transitions in the visible spectral range should be of the order of $2{\cdot}10^{-4}$. In reality the NOA of *f-f* transitions rich values of about 0.1 [1,5]. The value (9) is also called the dissymmetry factor, having in mind that the NOA should be proportional to the noncentro-symmetrical distortions. However we see that this is valid only for the parity allowed transitions. Fig. 10 demonstrates the NOA as a function of transitions intensity based on the Table 1 data. Predicted above inverse correlation between the NOA and the intensity of *f-f* transitions is seen. In view of this feature and basing on the Eq. (9), it is possible to suppose that more suitable characteristic of the real optical activity and of the dissymmetry of the local environment of the active ion in the case of *f-f* transitions can be circular dichroism Δf itself, i. e., numerator of fraction (9) (see Table 1). This value, indeed, does not correlate with the intensity of *f-f* transitions. However, the great variety of the NCD values both of absorption bands and of single lines (Tables 1 and 3) shows

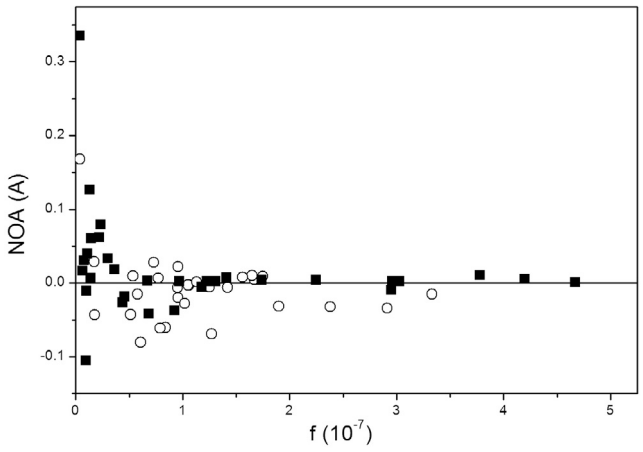

Fig. 10. NOA of *f-f* transitions as a function of the transitions oscillator strengths. Circles correspond to transitions from the ground state, squares correspond to transitions from the upper states of the ground multiplet.

that these values also can not be the characteristic of the dissymmetry. The NCD can characterize the local dissymmetry when we compare identical electron transitions in different compounds.

According to said above, already the little intensity of the vibronic transitions is a cause of the large NOA (A). However, the vibronic nature of transitions can give additional contribution into the NOA. In crystals with the center of inversion, odd vibrations mix wave functions of the opposite parity and so the vibrational repetitions of the parity forbidden electron transition become allowed (Herzberg–Teller interaction). Even vibrations mix wave functions of the same parity and therefore they can create repetitions of already allowed transitions. Intensities of such vibrational repetitions of the purely electronic transition are proportional to the Stokes losses during the vibronic transitions. Majority of the rare earth compounds have no center of inversion (mentioned above crystals including) and the *f-f* transitions are allowed due to the static odd distortions and are purely electronic ones. Conception of even and odd vibrations, strictly speaking, loses sense in such crystals, but the vibrations can be decomposed into odd and even parts. However, the vibrations partially preserve the mentioned properties, because deviation from the centro symmetrical structure is small. Thus, the mainly odd vibrations admix wave functions of the opposite parity and increase intensity of *f-f* transitions but do not increase the circular dichroism. The mainly even vibrations, on the contrary, admix wave functions of the same parity and do not increase intensity of *f-f* transitions but increase the circular dichroism. This can be one more origin of the particularly large NOA of the vibronic transitions. Additionally, the electron-vibrational interaction and covalency of bonds can increase delocalization of the electron wave functions and can additionally increase the NOA.

Er^{3+} and Ho^{3+} ions in $ErAl_3(BO_3)_4$ [13] and in $HoAl_3(BO_3)_4$ [12] crystals, respectively, are in the D_3 symmetry positions. In this symmetry p^x transforms according to E irreducible representation and the coordinate z – according to A_2 irreducible representation. Then the function zp^x, giving NOA, transforms according to

$$\Gamma(zp^x) = A_2 \times E = E \tag{11}$$

representation. Consequently, the symmetry selection rules for the NOA coincide with those for the α-polarized absorption (Tables 2 and 4), and all symmetry allowed transitions (the *f-f* transitions including) can have NOA. Similar situation takes place also in other uniaxial crystals.

It is known that intensity of the parity forbidden *f-f* transitions cannot be reliably found totally theoretically, and it is described by the semi-empirical Judd-Ofelt theory [48–50]. In the network of this theory, practically all *f-f* transitions are partially allowed (if there is no center of inversion) due to the selection rule: $\Delta J \leq \lambda$ (λ = 2, 4, 6), where J is the total momentum of the ion. In particular, all transitions studied in the present work are allowed in this approximation. Matrix elements $(zp^x)_{if}$, characterizing the NCD, probably, can be found theoretically for the *f-f* transitions, since for these transitions they are parity allowed. For the parity allowed transitions situation is opposite.

It is known that intensity and NOA of allowed transitions should not depend practically on temperature [35]. However our experiments [13] have shown that integral NOA of *f-f* absorption bands

Table 4
Selection rules for electric dipole transitions between non Kramers states in D_3 symmetry.

	A_1	A_2	E
A_1	–	π	$\sigma(\alpha)$
A_2	π	–	$\sigma(\alpha)$
E	$\sigma(\alpha)$	$\sigma(\alpha)$	π,$\sigma(\alpha)$

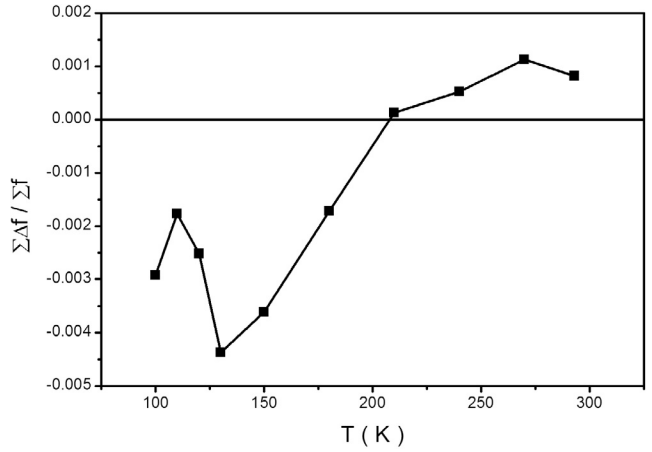

Fig. 11. NOA of sum of all studied absorption bands. Values of Δf and f at room temperature are presented in Table 3.

strongly depend on temperature and even change sign at some temperatures. NOA of sum of transitions is the ratio of integral of the NCD over all studied spectral range and integral of absorption over the same spectral range. Using measurements of Ref. [13], we have found temperature dependence of the NOA of sum of absorption bands presented in Table 3 (see Fig. 11). It is not zero and depends on temperature. Not monotonic temperature dependence is probably caused by the local structural distortions in the excited states. Thus, the sum rule is not fulfilled at least for the studied sum of *f-f* transitions. What can be the reason of such behavior of *f-f* transitions?

f–f transitions are allowed due to admixture of states with opposite parity to 4*f*-states by static or dynamic odd components of crystal field (CF). Let us consider an admixture of states with the opposite parity only to an excited 4*f*-state. This admixed J'_F state should also satisfy the total angular-momentum selection rule for the transition to be allowed:

$$|J'_F - J_I| \leqslant 1, \tag{12}$$

where J_I is the ground state total angular-momentum. According to (12) we have actually minimum three allowed transitions with their own intensities and optical activities. Intensities are summed up, while activities can have different signs. Ratio of the contributions strongly depends on details of the local symmetry of the Er^{3+} ion position, especially on the odd components of the crystal field. Additionally, this ratio changes with temperature because of redistribution of population of components of the ground multiplet crystal field splitting.

4. Summary

Absorption and NCD spectra of $ErAl_3(BO_3)_4$ single crystal were measured at 90 K in the range of 10,000–28,200 cm^{-1}. The spectra were decomposed on the Lorentz shape components and the NOA of the individual *f-f* transitions were found. The NCD spectrum permitted us to find out a splitting of one of the transitions which is impossible for the Kramers doublets. This splitting we refer to existence of two non equivalent positions of Er^{3+} ion in the corresponding excited state due to the local decrease of the crystal symmetry in this state. Very large NOA of a vibronic line was revealed. This phenomenon was accounted for, basing on the new quantum mechanical formula for the NOA of electron transitions. In contrast to the traditional one, it is consistent with the phenomenological theory. In particular, it contains the light wave number in the explicit form and the NOA of the electric dipole transitions do not contain matrix elements of the magnetic dipole operator. The theory has shown the principle difference of properties of the NOA of electric-dipole allowed and parity forbidden *f-f* transitions. In particular, NOA of *f-f* transitions should be and really is on the average much larger than that of allowed transitions. The theory has predicted inverse correlation between the NOA and intensity for the parity forbidden transitions. The experimental results confirmed such inverse correlation. The sum rule is not fulfilled for the studied *f-f* transitions.

Acknowledgements

The work was supported by the Russian Foundation for Basic Researches grant 16-02-00273 and by the President of Russia grant No Nsh-7559.2016.2.

References

[1] R. Berardozzi, L. Di Bari, Optical activity in the near-ir region: the λ = 980 nm multiplet of chiral Yb^{3+} complexes, ChemPhysChem 16 (2015) 2868–2875.
[2] L. Alyabyeva, V. Burkov, O. Lysenko, B. Mill, Absorption and circular-dichroism spectra of $LaBGeO_5$ crystal doped with Pr^{3+} and Ho^{3+} ions, Opt. Mater. 34 (2012) 803–806.
[3] D. Shirotani, H. Sato, K. Yamanari, S. Kaizaki, Electronic circular dichroism in the 4f–4f transitions of a series of cesium tetrakis (+)-3-heptafluorobutyrylcamphorate Ln (III) complexes, Dalton Trans. 41 (2012) 10557–10567.
[4] V.I. Burkov, O.A. Lysenko, B.V. Mill, Absorption and circular dichroism spectra of $La_3Ga_5SiO_{14}$ crystals doped with Pr^{3+}, Ho^{3+}, and Er^{3+} Ions, Crystallogr. Rep. 55 (2010) 983–989.
[5] V.I. Burkov, A.V. Butashin, E.V. Fedotov, A.F. Konstantinova, I.A. Gudim, Circular dichroism of some Nd-doped crystals of the langasite family, Crystallogr. Rep. 50 (2005) 954–960.
[6] V.I. Burkov, A.V. Egorysheva, A.Y. Vasil'ev, Y.F. Kargin, V.M. Skorikov, Absorption and circular dichroism spectra of $Bi_{12}SiO_{20}$ <Nd> crystals, Inorg. Mater. 38 (2002) 1035–1039.
[7] L. Fluyt, I. Couwenberg, H. Lambaerts, K. Binnemans, C. Görller-Walrand, Magnetic circular dichroism of $Na_3Nd(ODA)_3{\cdot}2NaClO4{\cdot}6H_2O$, J. Chem. Phys. 105 (1996) 6117–6127.
[8] K.A. Schoene, J.R. Quagliano, F.S. Richardson, Optical absorption and circular dichroism spectra, transition line strengths, and crystal-field analysis of the Er^{3+} $4f^{11}$ electronic energy-level structure in trigonal $Na_3[Er(C_4H4O_5)_3]$ $2NaClO_4{\cdot}6H_2O$, Inorg. Chem. 30 (1991) 3803–3812.
[9] F.S. Richardson, Chiroptical spectroscopy of lanthanide complexes, J. Less-Common Metals 149 (1989) 161–177.
[10] S. Misumi, T. Isobe, H. Furuta, Effect of pH on the circular dichroism (CD)-sensitive transitions of some lanthanoid (III) complexes and "Pseudo CD-sensitive Transitions" of europium (III) and terbium (III) complexes, Bul. Chem. Soc. Jupan 47 (1974) 421–423.
[11] S. Misumi, S. Kida, T. Isobe, Y. Nishida, H. Furuta, The "Circular Dichroism-sensitive Band" in the optical absorption of the lanthanide (III) complexes with some optically active ligands, Bul. Chem. Soc. Japan 42 (1969) 3433–'.
[12] A.V. Malakhovskii, A.L. Sukhachev, V.V. Sokolov, I.A. Gudim, Giant natural circular dichroism of vibronic transitions in HoAl3(BO3)4, JETP Lett. 102 (2015) 493–495.
[13] A.V. Malakhovskii, A.L. Sukhachev, V.V. Sokolov, T.V. Kutsak, V.S. Bondarev, I.A. Gudim, Magneto-optical activity of f–f transitions in $ErFe_3(BO_3)_4$ and $ErAl_3(BO_3)_4$ single crystals, J. Magn. Magn. Mater. 384 (2015) 255–265.
[14] Y.J. Chen, Y.F. Lin, X.H. Gong, Q.G. Tan, Z.D. Luo, Y.D. Huang, 2.0 W diode-pumped Er:Yb:$YAl_3(BO_3)_4$ laser at 1.5-1.6 mum, Appl. Phys. Lett. 89 (2006) 241111–241113.
[15] N.I. Leonyuk, V.V. Maltsev, E.A. Volkova, O.V. Pilipenko, E.V. Koporulina, V.E. Kisel, N.A. Tolstik, S.V. Kurilchik, N.V. Kuleshov, Crystal growth and laser properties of new $RAl_3(BO_3)_4$ (R = Yb, Er) crystals, Opt. Mater. 30 (2007) 161–163.
[16] Y. Chen, Y. Lin, X. Gong, J. Huang, Z. Luo, Y. Huang, Acousto-optic Q-switched self-frequency-doubling Er:Yb:$YAl_3(BO_3)_4$ laser at 800 nm, Opt. Lett. 37 (2012) 1565–1567.
[17] P. Dekker, J.M. Dawes, J.A. Piper, Y.G. Liu, J.Y. Wang, 1.1 W CW self-frequency-doubled diode-pumped Yb:$YAl_3(BO_3)_4$ laser, Opt. Commun. 195 (2001) 431–436.
[18] E. Cavalli, A. Speghini, M. Bettinelli, M.O. Ramirez, J.J. Romero, L.E. Bausa, J.G. Sole, Luminescence of trivalent rare earth ions in the yttrium aluminium borate non-linear laser crystal, J. Lumin. 102 (2003) 216–219.
[19] V. Singh, V.K. Rai, N. Singh, M.S. Pathak, M. Rathaiah, V. Venkatramu, R. Patel, P. K. Singh, S.J. Dhoble, Visible upconversion in Er^{3+}/Yb^{3+} co-doped $LaAlO_3$ phosphors, Spectrochim. Acta Part A: Molec. Biomol. Spectrosc. 171 (2017) 229–235.
[20] D. Kasprowicz, P. Głuchowski, M.G. Brik, M.M. Makowski, M. Chrunik, A. Majchrowski, Visible and near-infrared up-conversion luminescence of KGd

$(WO_4)(2)$ micro-crystals doped with Er^{3+}, Tm^{3+}, Ho^{3+} and Yb^{3+} ions, J. Alloys Compd. 684 (2016) 271–281.
[21] C.R. Kesavulu, H.J. Kim, S.W. Lee, J. Kaewkhao, N. Wantana, S. Kothan, S. Kaewjaeng, Influence of Er^{3+} ion concentration on optical and photoluminescence properties of Er^{3+}-doped gadolinium-calcium silica borate glasses, J. Alloys and Compd. 683 (2016) 590–598.
[22] S. Ray, R. Adhikari, G. Gyawali, B. Joshi, Y.K. Kshetri, C. Regmi, K. Tripathi, S. Lee, Plasmon and upconversion behavior in Ag–$BaMoO_4$: Er^{3+}/Yb^{3+} microcrystals, J. Nanosci. Nanotechnol. 16 (2016) 11645–11651.
[23] A. Baraldi, R. Capelletti, N. Magnani, M. Mazzera, E. Beregi, I. Földvári, Spectroscopic investigation and crystal field modelling of Dy^{3+} and Er^{3+} energy levels in yttrium aluminium borate (YAB) single crystals, J. Phys.: Condens. Matter 17 (2005) 6245–6255.
[24] M. Dammak, Crystal-field analysis of Er^{3+} ions in yttrium aluminium borate (YAB) single crystals, J. Alloys Comp. 393 (2005) 51–56.
[25] I. Földvári, E. Beregi, R. Capelletti, A. Baraldi, Visible range optical absorption of Er^{3+} ions in yttrium aluminum borate (YAB) crystals, Phys. Stat. Sol. (c) 2 (2005) 260–263.
[26] W. You, Y. Huang, Y. Chen, Y. Lin, Z. Luo, The effect of Yb^{3+} concentrations on the properties of Yb, Er: $YAl_3(BO_3)_4$ crystals, Physica B 405 (2010) 34–37.
[27] A.V. Malakhovskii, T.V. Kutsak, A.L. Sukhachev, A.S. Aleksandrovsky, A.S. Krylov, I.A. Gudim, M.S. Molokeev, Spectroscopic properties of $ErAl_3(BO_3)_4$ single crystal, Chem. Phys. 428 (2014) 137–143.
[28] I.A. Gudim, E.V. Eremin, V.L. Temerov, Flux growth and spin reorientation in trigonal $Nd_{1-x}Dy_xFe_3(BO_3)_4$ single crystals, J. Cryst. Growth 312 (2010) 2427–2430.
[29] K. Teshima, Y. Kikuchi, T. Suzuki, S. Oishi, Growth of $ErAl_3(BO_3)_4$ Single Crystals from a $K_2Mo_3O_{10}$ Flux, Cryst. Growth Des. 6 (2006) 1766–1768.
[30] A.V. Malakhovskii, S.L. Gnatchenko, I.S. Kachur, V.G. Piryatinskaya, A.L. Sukhachev, I.A. Gudim, Optical and magneto-optical properties of $Nd_{0.5}Gd_{0.5}Fe_3(BO_3)_4$ single crystal in the near IR spectral region, J. Alloys Compd. 542 (2012) 157–163.
[31] A.A. Kaminskii, Crystalline Lasers: Physical Processes and Operating Schemes, CRC Press, New York, London, Tokyo, 1996.
[32] A.V. Malakhovskii, V.V. Sokolov, I.A. Gudim, Optical and magneto-optical spectra and electron structure of $ErAl_3(BO_3)_4$ single crystal, J. Alloys Compd. 698 (2017) 364–374.
[33] F.S. Richardson, Selection rules for lanthanide optical activity, Inorg. Chem. 19 (1980) 2806–2812.
[34] F.S. Richardson, T.R. Faulkner, Optical activity of the *f–f* transitions in trigonal dihedral (D_3) lanthanide (III) complexes. I. Theory, J. Chem. Phys. 76 (1982) 1595–1606.
[35] J.D. Saxe, T.R. Faulkner, F.S. Richardson, Optical activity of the *f–f* transitions in trigonal dihedral (D_3) lanthanide (III) complexes. II. Calculations, J. Chem. Phys. 76 (1982) 1607–1623.
[36] W. Moffit, A. Moscovitz, Optical activity in absorbing media, J. Chem. Phys. 30 (1959) 648–660.
[37] A.V. Malakhovskii, A.L. Sukhachev, A.A. Leont'ev, V.L. Temerov, Magnetic and natural optical activity of *f–f* transitions in multiferroic $Nd_{0.5}Gd_{0.5}Fe_3(BO_3)_4$, Phys. Sol. State 58 (2016) 952–958.
[38] S.A. Klimin, D. Fausti, A. Meetsma, L.N. Bezmaternykh, P.H.M. van Loosdrecht, T.T.M. Palstra, Evidence for differentiation in the iron-helicoidal chain in $GdFe_3(BO_3)_4$, Acta Crystallogr. B 61 (2005) 481–485.
[39] B.J. Campbell, H.T. Stokes, D.E. Tanner, D.M. Hatch, ISODISPLACE: a web-based tool for exploring structural distortions, J. Appl. Crystallography 39 (2006) 607–614.
[40] J.A. Schellman, Circular dichroism and optical rotation, Chem. Rev. 75 (1975) 323–331.
[41] D.J. Caldwell, H. Eyring, The Theory of Optical Activity, Wiley (Interscience), New York, 1971.
[42] D.J. Caldwell, H. Eyring, Models in Optical Activity. Theor. Chem. Advances, a. Persp. Acad. Press, 1975, v. 1, pp. 53–116.
[43] K.E. Gunde, G.W. Burdicka, F.S. Richardson, Chirality-dependent two-photon absorption probabilities and circular dichroic line strengths: theory, calculation and measurement, Chem. Phys. 208 (1996) 195–219.
[44] M. Krykunov, J. Autschbach, Calculation of origin-independent optical rotation tensor components in approximate time-dependent density functional theory, J. Chem. Phys. 125 (2006), 034102(1-10).
[45] H.-G. Kuball, J. Altschuh, Optical activity of oriented molecules. comparison of the optical rotatory dispersion and the circular dichroism through the Kramers-Kronig transform, Chem. Phys. Letters 87 (1982) 599–603.
[46] V.M. Agranovich, V.L. Ginsburg, Crystal Optics with the Space Dispersion and Theory of Excitons, Nauka, Moscow, 1979 (in Russian).
[47] J. Snir, J. Schellman, Optical activity of oriented helixes. Quadrupole contributions, J. Phys. Chem. 77 (1973) 1653–1661.
[48] B.R. Judd, Optical absorption intensities of rare-earth ions, Phys. Rev. 127 (1962) 750–761.
[49] G.S. Ofelt, Intensities of crystal spectra of rare-earth ions, J. Chem. Phys. 37 (1962) 511–520.
[50] R.D. Peacock, The intensities of lanthanide *f-f* transitions, Struct. Bond. 22 (1975) 83–122.